Model reduction, data-based and advanced discretization in computational mechanics

Advanced parametric space-frequency separated representations in structural dynamics: A harmonic–modal hybrid approach

Muhammad Haris Malik [a,*], Domenico Borzacchiello [b], Jose Vicente Aguado [b], Francisco Chinesta [c]

[a] *Department of Mechanical Engineering, DHA Suffa University Off Khayaban-e-Tufail, Phase VII(Ext) DHA, Karachi-75500, Pakistan*
[b] *ICI – Institut de calcul intensif & ESI GROUP Chair, École centrale de Nantes, 1, rue de la Noë, 44300 Nantes, France*
[c] *PIMM Laboratory & ESI GROUP Chair, ENSAM ParisTech, 151, boulevard de l'Hôpital, 75013 Paris, France*

A B S T R A C T

This paper is concerned with the solution to structural dynamics equations. The technique here presented is closely related to Harmonic Analysis, and therefore it is only concerned with the long-term forced response. Proper Generalized Decomposition (PGD) is used to compute space-frequency separated representations by considering the frequency as an extra coordinate. This formulation constitutes an alternative to classical methods such as Modal Analysis and it is especially advantageous when parametrized structural dynamics equations are of interest. In such case, there is no need to solve the parametrized eigenvalue problem and the space-time solution can be recovered with a Fourier inverse transform. The PGD solution is valid for any forcing term that can be written as a combination of the considered frequencies. Finally, the solution is available for any value of the parameter. When the problem involves frequency-dependent parameters the proposed technique provides a specially suitable method that becomes computationally more efficient when it is combined with a modal representation.

© 2018 Académie des sciences. Published by Elsevier Masson SAS. All rights reserved.

1. Introduction

Governing equations in solid dynamics are usually formulated either in the time or in the frequency domains. The former is preferred when calculating transient responses, whereas the frequency approach is an appealing choice for calculating forced responses. Both approaches have been extensively used and described in many reference books, as for example [1].

Formulations in the frequency domain are based on the computation of a suitable approximation basis, the so-called modal basis, that allows very efficient time integrations by decoupling the generalized degrees of freedom (the ones associated with the different modes). The determination of the said basis is related to the solution to an eigenvalue problem, as illustrated in the following sections. Limiting the computation of the eigenvectors to those that are related to the highest eigenvalues can lead to efficient strategies for reduced-order approximations.

* Corresponding author.
  E-mail addresses: haris.malik@dsu.edu.pk (M.H. Malik), domenico.borzacchiello@ec-nantes.fr (D. Borzacchiello), jose.aguado-lopez@ec-nantes.fr (J.V. Aguado), Francisco.CHINESTA@ensam.edu (F. Chinesta).

As will be discussed in the next section, problems become a bit more complex in the case of parametrized dynamics, and more concretely when those parameters are assumed to be depending on the frequency. In this case, frequency-based modeling seems more appropriate than its time counterpart, provided that the functional forms expressing the parameters dependence on the frequency are compatible with the use of space-frequency-parameter separated variable representation, which represents the core idea of model order reduction.

Thus new proposals able to address parametrized dynamics, with parameters depending on the frequency in general forms and able to proceed under the real-time constraint for evaluating the time response of complex structures under dynamical loadings, could constitute a useful framework for addressing a variety of applicative problems.

In this paper we revisit, starting from standard linear dynamics in the next section, some relevant and timely questions concerning the use of parametric models and their frequency dependence, proving then that, combining modal and harmonic analyses, both defined in the frequency domain, leads to a very powerful solution procedure for parametric frequency-dependent dynamic systems.

2. Standard dynamics at a glance

The general semi-discrete form of linear solid dynamics equations writes

$$\mathbf{M}\frac{\mathrm{d}^2\mathbf{U}(t)}{\mathrm{d}t^2} + \mathbf{C}\frac{\mathrm{d}\mathbf{U}(t)}{\mathrm{d}t} + \mathbf{K}\mathbf{U}(t) = \mathbf{F}(t) \tag{1}$$

where $\mathbf{M}$, $\mathbf{C}$ and $\mathbf{K}$ are respectively the mass, damping and stiffness matrices, $\mathbf{U}$ the vector that contains the nodal displacements, and $\mathbf{F}$ the nodal excitations (forces). This equation can be obtained through any suitable mesh-based discretization technique like, for instance, the Finite Element Method.

The main drawback related to the time integration of Eq. (1) lies in the necessity of solving a linear system (usually of very large size) at each time step, in particular when some of these matrices change in time for a variety of reasons (including time-dependent behavior or nonlinearities) and need to be reassembled at each time step.

Loads can be easily expressed in the frequency domain. In what follows, we consider without loss of generality the simplest scenario: $\mathbf{F}(t) = \mathbf{f}g(t)$, with $\|\mathbf{f}\| = 1$. The time function $g(t)$ can be expressed from the superposition of harmonic functions $\mathrm{e}^{\mathrm{i}\omega t}$, with ω the circular frequency and $\mathrm{i} = \sqrt{-1}$. If we assume a single frequency harmonic excitation, $g(t) = \mathrm{e}^{\mathrm{i}\omega t}$, the response of a linear solid is expected having the same frequency but exhibiting a certain phase angle θ, i.e. $\mathbf{U}(t) = \overline{\mathbf{U}}\mathrm{e}^{\mathrm{i}\omega t + \mathrm{i}\theta}$, where $\overline{\mathbf{U}}$ is the vector containing the amplitude of the nodal displacements. This vector can be rewritten as $\mathbf{U}(t) = \overline{\mathbf{U}}\mathrm{e}^{\mathrm{i}\omega t + \mathrm{i}\theta} = \mathbb{U}\mathrm{e}^{\mathrm{i}\omega t}$, where now $\mathbb{U} = \overline{\mathbf{U}}\mathrm{e}^{\mathrm{i}\theta}$ denotes a vector of complex entries, with $\mathbb{U} = \mathbf{U}_r + \mathrm{i}\mathbf{U}_i$, where $\mathbf{U}_r$ and $\mathbf{U}_i$ are respectively the real and imaginary parts of $\mathbb{U}$.

By introducing $\mathbf{F}(t) = \mathbf{f}\mathrm{e}^{\mathrm{i}\omega t}$ and $\mathbf{U}(t) = \mathbb{U}\mathrm{e}^{\mathrm{i}\omega t}$ into Eq. (1) it results in the frequency-based description of solid dynamics

$$\left(-\omega^2\mathbf{M} + \mathrm{i}\omega\mathbf{C} + \mathbf{K}\right)\mathbb{U} = \mathbf{f} \tag{2}$$

where the exponential factor $\mathrm{e}^{\mathrm{i}\omega t}$ was eliminated from both members.

If damping vanishes, i.e. $\mathbf{C} = \mathbf{0}$, and one focuses on the free response of the mechanical system, i.e. $\mathbf{f} = \mathbf{0}$, then Eq. (2) reduces to:

$$\mathbf{K}\mathbb{U} = \omega^2\mathbf{M}\mathbb{U} \tag{3}$$

that defines an eigenproblem that results in the eigenmodes $\mathbb{U}_i$ and the associated eigenfrequencies ω_i^2. Eigenmode $\mathbb{U}_i$ scaled from some normalization condition is called normal mode and is noted by $\boldsymbol{\phi}_i$. It is usual to normalize eigenmodes according to $\boldsymbol{\phi}_i^\mathsf{T}\mathbf{M}\boldsymbol{\phi}_i = M_i = 1$, from which it results $\boldsymbol{\phi}_i^\mathsf{T}\mathbf{K}\boldsymbol{\phi}_i = K_i = \omega_i^2$, where M_i and K_i are known as modal mass and modal stiffness, respectively. If normal modes are placed in the columns of matrix $\mathbf{P}$, we could express $\mathbb{U}$ in the orthonormal basis defined by the normal modes involving coefficients $\boldsymbol{\xi}(\mathbf{t})$, according to

$$\mathbb{U} = \mathbf{P}\boldsymbol{\xi}(t) \tag{4}$$

Now, by inserting (4) into Eq. (1), premultiplying by the transpose of $\mathbf{P}$ and taking into account the orthogonality conditions $\boldsymbol{\phi}_j^\mathsf{T}\mathbf{M}\boldsymbol{\phi}_i = 0$ and $\boldsymbol{\phi}_j^\mathsf{T}\mathbf{K}\boldsymbol{\phi}_i = 0$ when $i \neq j$, it results

$$\mathbf{I}\frac{\mathrm{d}^2\boldsymbol{\xi}(t)}{\mathrm{d}t^2} + \mathbf{P}^\mathsf{T}\mathbf{C}\mathbf{P}\frac{\mathrm{d}\boldsymbol{\xi}(t)}{\mathrm{d}t} + \mathbf{diag}(\omega_i^2)\boldsymbol{\xi}(t) = \mathbf{P}^\mathsf{T}\mathbf{F}(t) \tag{5}$$

where $\mathbf{I}$ is the unit matrix.

When damping vanishes, i.e. $\mathbf{C} = \mathbf{0}$, the previous equation reduces to a linear system of uncoupled second order ordinary differential equations.

When damping applies, the matrix $\tilde{\mathbf{C}} \equiv \mathbf{P}^\mathsf{T}\mathbf{C}\mathbf{P}$ is not in general diagonal, compromising the efficiency of modal analysis. To circumvent this issue, different diagonalization procedures have been proposed and widely used. Two usual diagonalization procedures are: (i) diagonalization by model damping that expresses $\tilde{\mathbf{C}} = \mathbf{diag}(2\zeta_i\omega_i)$, where ζ_i denotes the damping ratio

for the i-th natural mode; and (ii) Rayleigh diagonalization by assuming $\mathbf{C} = a_0\mathbf{M} + a_1\mathbf{K}$ results in $\tilde{\mathbf{C}} = \mathbf{diag}(a_0 + a_1\omega_i^2) = \mathbf{diag}(2\zeta_i\omega_i)$, with $\zeta_i = \frac{1}{2}\left(\frac{a_0}{\omega_i} + a_1\omega_i\right)$. These choices imply approximations whose validity and accuracy must be checked.

A more precise route consists in extracting the modes from the solution to the quadratic complex eigenproblem:

$$\left(\mathbf{K} + i\omega\mathbf{C} - \omega^2\mathbf{M}\right)\mathbb{U} = \mathbf{0} \tag{6}$$

However, many times models involve parametric damping, that is, damping depending on some parameters grouped in vector $\boldsymbol{\mu}$, $\mathbf{C}(\boldsymbol{\mu})$, and in that case the resolution of parametric quadratic eigenproblems remains a tricky issue [2,3]. Similar issues arise in other fields of science and engineering as well, for example, [4] and aerodynamic loadings of suspension bridges [5].

When one is interested in solving problems with parametric damping, an efficient strategy is to avoid direct time integrations or time integrations based on modal analysis, in favor of a purely harmonic approach, making use of Eq. (2).

In what follows, we assume that the applied load can be written from the superposition of harmonic functions of angular frequency ω

$$g(t) = \int_{-\infty}^{\infty} \mathcal{G}(\omega)e^{i\omega t}d\omega \tag{7}$$

where $\mathcal{G}(\omega)$ represents the content of each harmonic $e^{i\omega t}$ in $g(t)$. In fact, $\mathcal{G}(\omega)$ is the Fourier transform of $g(t)$

$$\mathcal{G}(\omega) \equiv \mathcal{F}(g(t)) = \int_{-\infty}^{\infty} g(t)e^{-i\omega t}dt \tag{8}$$

In general $\mathcal{G}(\omega < \omega^-) = \mathcal{G}(\omega > \omega^+) \approx 0$, that is,

$$g(t) \approx \int_{\omega^-}^{\omega^+} \mathcal{G}(\omega)e^{i\omega t}d\omega \tag{9}$$

which implies that Eq. (2) must be solved for any value of $\omega \in \mathcal{I} = [\omega^-, \omega^+]$

$$\left(-\omega^2\mathbf{M} + i\omega\mathbf{C} + \mathbf{K}\right)\mathbb{U}(\omega) = \mathbf{f} \tag{10}$$

leading to the parametric solution $\mathbb{U}(\omega)$. This characterizes the linear behavior of a system and describes a generalized solution by virtue of the superposition principle

$$\mathbf{U}(t) = \int_{\omega^-}^{\omega^+} \mathcal{G}(\omega)\,\mathbb{U}(\omega)\,e^{i\omega t}\,d\omega \tag{11}$$

The main drawback of that approach is the necessity of solving a linear system related to the solution to Eq. (10) for each value of ω involved in the discrete inverse transform (11). Therefore, the computational cost increases with the frequency interval length $\Delta\omega = |\omega^+ - \omega^-|$ and with the signal's resolution. For this reason, modal analysis is usually preferred to harmonic analysis.

In the general parametric case, mass, damping, and stiffness matrices can depend on a series of parameters grouped in the vector $\boldsymbol{\mu}$, i.e. $\mathbf{M}(\boldsymbol{\mu})$, $\mathbf{C}(\boldsymbol{\mu})$ and $\mathbf{K}(\boldsymbol{\mu})$, leading to a parametric eigenproblem [2], [3], implying an even higher computational effort, in case a fully parametric solution in explicit form is sought. On the other hand, the use of harmonic analysis requires solving Eq. (10) for each frequency ω and each possible choice of the parameters $\boldsymbol{\mu}$, $\mathbb{U}(\omega; \boldsymbol{\mu})$ to finally compute the discrete sum related to

$$\mathbf{U}(t; \boldsymbol{\mu}) = \int_{\omega^-}^{\omega^+} \mathcal{G}(\omega)\,\mathbb{U}(\omega; \boldsymbol{\mu})\,e^{i\omega t}\,d\omega \tag{12}$$

for any choice of the parameters $\boldsymbol{\mu}$.

For instance, if only two parameters $\boldsymbol{\mu}^\mathsf{T} = (\mu_1, \mu_2)$ are considered, a parametric sweep including a hundred points per parameter will produce 10^4 samples. Furthermore, if we assume 10^4 discrete frequencies involved in the reconstruction of $g(t)$, the calculation of the parametric solution $\mathbb{U}(\omega_i; \boldsymbol{\mu})$ requires solving 10^8 linear systems.

The use of the Proper Generalized Decomposition (PGD), largely considered in our former works [6–10], allows solving the parametric model

$$\left(-\omega^2 \mathbf{M}(\boldsymbol{\mu}) + i\omega \mathbf{C}(\boldsymbol{\mu}) + \mathbf{K}(\boldsymbol{\mu})\right) \mathbb{U}(\omega, \boldsymbol{\mu}) = \mathbf{f} \tag{13}$$

by assuming the separated representation

$$\mathbb{U}(\omega, \mu_1, \mu_2) \approx \sum_{k=1}^{N} \mathbf{Z}_k W_k(\omega) \mathcal{M}_k^1(\mu_1) \mathcal{M}_k^2(\mu_2) \tag{14}$$

where $\mathbf{Z}_k$ is a vector of nodal displacements and $W_k(\omega)$, $\mathcal{M}_k^1(\mu_1)$ and $\mathcal{M}_k^2(\mu_2)$ are functions that depend on the extra-coordinates ω, μ_1 and μ_2, respectively. The construction of the separated representation (14) implies the resolution of a number of linear systems scaling with the number of terms involved in the finite sum, i.e. in the order of N linear systems (N being in general of few tens).

In soil mechanics [11], the damping is assumed scaling with the inverse of frequency. The interested reader can refer to [12], which analyzes the theoretical consequences of assuming a frequency-dependent dashpot parameter. In [12], it was proved that, even if such a choice succeeded to fit experimental data, when coming back to the time space, causality is lost, and then the resulting expressions in the time domain were called *non-equations*. However, it is important to note that, even when considering complex nonlinear frequency-dependent damping $\mathbf{C}(\omega)$ in Eq. (2), the problem in the frequency domain remains linear because here the frequency is a model parameter (or an extra-coordinate model within the PGD framework).

3. Harmonic analysis from a separated representation perspective

We consider the space-frequency formulation

$$\left(-\omega^2 \mathbf{M} + i\omega \mathbf{C} + \mathbf{K}\right) \mathbb{U}(\omega) = \mathbf{f} \tag{15}$$

and look for its space-frequency separated representation

$$\mathbb{U}(\omega) \approx \sum_{k=1}^{N} \mathbf{Z}_k W_k(\omega) \tag{16}$$

Space-time and space-frequency separated representations were used for solving dynamics problems [13,14]. In [15], the authors extended such a decomposition for efficiently addressing parabolic problems. Finally, parameters were also included as extra-coordinates in such a representation [15–17].

For that purpose, we consider the usual integral form considered when applying the PGD constructor

$$\int_{\mathcal{I}} \mathbb{U}^{*\mathsf{T}}(\omega) \left(-\omega^2 \mathbf{M} + i\omega \mathbf{C} + \mathbf{K}\right) \mathbb{U}(\omega) \, d\omega = \int_{\mathcal{I}} \mathbb{U}^{*\mathsf{T}}(\omega) \mathbf{f} \, d\omega \tag{17}$$

assuming at iteration n the solution $\mathbb{U}^{n-1}(\omega)$ is known, and looking for $\mathbb{U}^n(\omega)$

$$\mathbb{U}^n(\omega) = \sum_{k=1}^{n-1} \mathbf{Z}_k W_k(\omega) + \mathbf{Z}_n W_n(\omega) \tag{18}$$

with the test function $\mathbb{U}^*(\omega)$ expressed from

$$\mathbb{U}^*(\omega) = \mathbf{Z}^* W_n(\omega) + \mathbf{Z}_n W^*(\omega) \tag{19}$$

Thus, Eq. (17) can be expressed at the present iteration as

$$\int_{\mathcal{I}} \mathbb{U}^{*\mathsf{T}}(\omega) \left(-\omega^2 \mathbf{M} + i\omega \mathbf{C} + \mathbf{K}\right) \mathbf{Z}_n W_n(\omega) \, d\omega =$$

$$\int_{\mathcal{I}} \mathbb{U}^{*\mathsf{T}}(\omega) \mathbf{f} \, d\omega - \int_{\mathcal{I}} \mathbb{U}^{*\mathsf{T}}(\omega) \left(-\omega^2 \mathbf{M} + i\omega \mathbf{C} + \mathbf{K}\right) \left(\sum_{k=1}^{n-1} \mathbf{Z}_k W_k(\omega)\right) \, d\omega \tag{20}$$

In order to solve the previous nonlinear problem, we consider an alternating direction fixed-point strategy that, by assuming known $\mathbf{Z}_n$, calculates W_n, from which $\mathbf{Z}_n$ is updated, and so on until reaching the iteration fixed point. Both steps are described below.

(i) Calculating $\mathbf{Z}_n$ by assuming known $W_n(\omega)$.

In that case the test function reads

$$\mathbb{U}^*(\omega) = \mathbf{Z}^* W_n(\omega) \tag{21}$$

from which Eq. (20) writes

$$\int_{\mathcal{I}} \mathbf{Z}^{*\mathsf{T}} W_n(\omega) \left(-\omega^2 \mathbf{M} + \mathrm{i}\omega \mathbf{C} + \mathbf{K}\right) \mathbf{Z}_n W_n(\omega) \, \mathrm{d}\omega =$$

$$\int_{\mathcal{I}} \mathbf{Z}^{*\mathsf{T}} W_n(\omega) \mathbf{f} \, \mathrm{d}\omega - \int_{\mathcal{I}} \mathbf{Z}^{*\mathsf{T}} W_n(\omega) \left(-\omega^2 \mathbf{M} + \mathrm{i}\omega \mathbf{C} + \mathbf{K}\right) \left(\sum_{k=1}^{n-1} \mathbf{Z}_k W_k(\omega)\right) \mathrm{d}\omega \tag{22}$$

By performing the frequency-dependent integrals:

$$\begin{cases} \alpha^\omega = \int_{\mathcal{I}} W_n^2(\omega)\omega^2 \, \mathrm{d}\omega \\ \beta^\omega = \int_{\mathcal{I}} W_n^2(\omega)\omega \, \mathrm{d}\omega \\ \gamma^\omega = \int_{\mathcal{I}} W_n^2(\omega) \, \mathrm{d}\omega \\ \delta^\omega = \int_{\mathcal{I}} W_n(\omega) \, \mathrm{d}\omega \\ \alpha_k^\omega = \int_{\mathcal{I}} W_n(\omega)\omega^2 W_k(\omega) \, \mathrm{d}\omega \\ \beta_k^\omega = \int_{\mathcal{I}} W_n(\omega)\omega W_k(\omega) \, \mathrm{d}\omega \\ \gamma_k^\omega = \int_{\mathcal{I}} W_n(\omega) W_k(\omega) \, \mathrm{d}\omega \end{cases} \tag{23}$$

Eq. (22) reduces to

$$\mathbf{Z}^{*\mathsf{T}} \left(-\alpha^\omega \mathbf{M} + \mathrm{i}\beta^\omega \mathbf{C} + \gamma^\omega \mathbf{K}\right) \mathbf{Z}_n = \mathbf{Z}^{*\mathsf{T}} \delta^\omega \mathbf{f} - \mathbf{Z}^{*\mathsf{T}} \sum_{k=1}^{n-1} \left(\left(-\alpha_k^\omega \mathbf{M} + \mathrm{i}\beta_k^\omega \mathbf{C} + \gamma_k^\omega \mathbf{K}\right) \mathbf{Z}_k\right) \tag{24}$$

which, being $\mathbf{Z}^*$ arbitrary, leads finally to the linear system

$$\left(-\alpha^\omega \mathbf{M} + \mathrm{i}\beta^\omega \mathbf{C} + \gamma^\omega \mathbf{K}\right) \mathbf{Z}_n = \tilde{\mathbf{f}} \tag{25}$$

with

$$\tilde{\mathbf{f}} = \delta^\omega \mathbf{f} - \sum_{k=1}^{n-1} \left(\left(-\alpha_k^\omega \mathbf{M} + \mathrm{i}\beta_k^\omega \mathbf{C} + \gamma_k^\omega \mathbf{K}\right) \mathbf{Z}_k\right) \tag{26}$$

that allows computing $\mathbf{Z}_n$.

(ii) Calculating $W_n(\omega)$ by assuming known $\mathbf{Z}_n$.

In that case, the test function reads

$$\mathbb{U}^*(\omega) = \mathbf{Z}_n W^*(\omega) \tag{27}$$

from which Eq. (20) writes

$$\int_{\mathcal{I}} \mathbf{Z}_n^{\mathsf{T}} W^*(\omega) \left(-\omega^2 \mathbf{M} + \mathrm{i}\omega \mathbf{C} + \mathbf{K}\right) \mathbf{Z}_n W_n(\omega) \, \mathrm{d}\omega =$$

$$\int_{\mathcal{I}} \mathbf{Z}_n^{\mathsf{T}} W^*(\omega) \mathbf{f} \, \mathrm{d}\omega - \int_{\mathcal{I}} \mathbf{Z}_n^{\mathsf{T}} W^*(\omega) \left(-\omega^2 \mathbf{M} + \mathrm{i}\omega \mathbf{C} + \mathbf{K}\right) \left(\sum_{k=1}^{n-1} \mathbf{Z}_k W_k(\omega)\right) \mathrm{d}\omega \tag{28}$$

By performing the matrix products:

$$\begin{cases} \alpha^z = \mathbf{Z}_n^{\mathsf{T}} \mathbf{M} \mathbf{Z}_n \\ \beta^z = \mathbf{Z}_n^{\mathsf{T}} \mathbf{C} \mathbf{Z}_n \\ \gamma^z = \mathbf{Z}_n^{\mathsf{T}} \mathbf{K} \mathbf{Z}_n \\ \delta^z = \mathbf{Z}_n^{\mathsf{T}} \mathbf{f} \\ \alpha_k^z = \mathbf{Z}_n^{\mathsf{T}} \mathbf{M} \mathbf{Z}_k \\ \beta_k^z = \mathbf{Z}_n^{\mathsf{T}} \mathbf{C} \mathbf{Z}_k \\ \gamma_k^z = \mathbf{Z}_n^{\mathsf{T}} \mathbf{K} \mathbf{Z}_k \end{cases} \tag{29}$$

Eq. (28) reduces to

$$
\int_{\mathcal{I}} W^*(\omega)\left(-\omega^2\alpha^z + i\omega\beta^z + \gamma^z\right) W_n(\omega)\, \mathrm{d}\omega = \int_{\mathcal{I}} W^*(\omega)\gamma^z\, \mathrm{d}\omega
$$
$$
- \int_{\mathcal{I}} W^*(\omega) \sum_{k=1}^{n-1}\left(\left(-\omega^2\alpha_k^z + i\omega\beta_k^z + \gamma_k^z\right) W_k(\omega)\right)\, \mathrm{d}\omega \tag{30}
$$

which, using the arbitrariness of W^*, leads to the algebraic equation

$$
\left(-\omega^2\alpha^z + i\omega\beta^z + \gamma^z\right) W_n(\omega) = h(\omega) \tag{31}
$$

with

$$
h(\omega) = \gamma^z - \sum_{k=1}^{n-1}\left(\left(-\omega^2\alpha_k^z + i\omega\beta_k^z + \gamma_k^z\right) W_k(\omega)\right) \tag{32}
$$

that allows calculating the function $W_n(\omega)$.

This procedure allows us to compute the functions $\mathbf{Z}_n$ and $W_n(\omega)$ in a greedy algorithm, in which the originally two-dimensional problem is broken down to the sequential solution to one-dimensional smaller problems. The enrichment process is stopped once the number of computed terms is enough to obtain the desired accuracy. A detailed numerical procedures and implementation aspects are presented in [9]. The separated representation of the nodal displacements $\mathbb{U}(\omega)$ resulting from the PGD method is given by Eq. (16).

Even if the problem is linear and is assumed to have a unique solution, the separated variables approximations is not unique since it can be computed in different *formats* depending on the numerical algorithm adopted for the construction of the solution. Indeed, the individual terms appearing in Eq. 16 can differ from one computational strategy to another, although they will sum to the same values. In order to obtain the most compact expression of the solution, regardless of the considered constructor, the Singular Value Decomposition (SVD) or its high-order counterpart, the so-called HOSVD, can be employed as a post-processing step. Recall that the SVD is optimal in terms of compactness, at least in two dimensions. Connections between SVD and PGD are described in [9].

3.1. Parametric harmonic analyses

If parameters are assumed as extra-coordinates, as is usual within the PGD framework [8], the computed parametric solution allows real-time simulation, optimization, inverse analyses, and simulation-based control in a very efficient way.

Parametric dynamics was addressed in [16,17]. If, for the sake of notational clarity, we consider a single parameter μ involved in the model and affecting the three terms of the momentum balance (mass, damping, and elastic terms), the dynamical problem reads

$$
\left(-\omega^2\mathcal{L}^m(\mu)\mathbf{M} + i\omega\mathcal{L}^c(\mu)\mathbf{C} + \mathcal{L}^k(\mu)\mathbf{K}\right)\mathbb{U}(\omega,\mu) = \mathbf{f} \tag{33}
$$

whose parametric solution is sought under the separated form

$$
\mathbb{U}(\omega,\mu) \approx \sum_{k=1}^{N} \mathbf{Z}_k W_k(\omega)\mathcal{M}_k(\mu) \tag{34}
$$

To construct the separated representation (34), we apply again the algorithm described in the previous section. In this case, each enrichment iteration n involves the solution to three one-dimensional problems. The first one is needed to compute space vectors $\mathbf{Z}_n$ and is related to the solution to a linear system of equations arising from the discretization of differential operators in space, while the computation of the modes $W_n(\omega)$ and $\mathcal{M}_m(\mu)$ only involves the solution to decoupled algebraic equations. For more details, the interested readers can refer to [6,18,19].

When considering many parameters $\mu_1,\cdots,\mu_p \equiv \boldsymbol{\mu}$, the solution, in its separated representation expression, reads

$$
\mathbb{U}(\omega,\boldsymbol{\mu}) \approx \sum_{k=1}^{N} \mathbf{Z}_k W_k(\omega)\mathcal{M}_k^1(\mu_1)\cdots\mathcal{M}_k^p(\mu_p) \tag{35}
$$

As a remark, it is often useful for efficient numerical implementation to consider an affine decomposition of the different operators appearing in Eq. (33)

$$\begin{cases} \mathbf{M}(\boldsymbol{\mu}) = \sum_{j=1}^{Q_m} \mathcal{L}_j^{m,1}(\mu_1)\cdots\mathcal{L}_j^{m,1}(\mu_p)\mathbf{M}_j \\[2mm] \mathbf{C}(\boldsymbol{\mu}) = \sum_{j=1}^{Q_c} \mathcal{L}_j^{c,1}(\mu_1)\cdots\mathcal{L}_j^{c,1}(\mu_p)\mathbf{C}_j \\[2mm] \mathbf{K}(\boldsymbol{\mu}) = \sum_{j=1}^{Q_k} \mathcal{L}_j^{k,1}(\mu_1)\cdots\mathcal{L}_j^{k,1}(\mu_p)\mathbf{K}_j \end{cases} \tag{36}$$

In cases in which it is not possible to enforce such a decomposition exactly, approximate decomposition techniques can be used [20,21].

4. A harmonic–modal hybrid – HMH – description for parametric frequency-dependent models

When damping is neglected, $\mathbf{C} = \mathbf{0}$, or when proportional damping is considered, $\mathbf{C} = a_0\mathbf{M} + a_1\mathbf{K}$, the single-parameter dynamic equation reads

$$\left(-\omega^2 \mathcal{L}^m(\mu)\mathbf{M} + \mathcal{L}^k(\mu)\mathbf{K}\right)\mathbb{U}(\omega,\mu) = \mathbf{f} \tag{37}$$

A particularly difficult situation is found when it is assumed that parameter μ depends on the frequency, as usually considered in soil dynamics, structural dynamics, and power-transmission dynamics [22].

In this case, assuming a frequency-dependent parameter $\mu(\omega)$ in the equation

$$\left(-\omega^2 \mathcal{L}^m(\mu(\omega))\mathbf{M} + \mathcal{L}^k(\mu(\omega))\mathbf{K}\right)\mathbb{U}(\omega,\mu) = \mathbf{f} \tag{38}$$

introduces a formal difficulty in establishing an equivalent formulation in the time domain. In fact, the inverse transformation to the time domain may imply the loss of causality. The appellation *non-equation* originated from this consideration [12].

In the case just described, time formulations are seldom employed, since traditional modal analysis based on the diagonalization of matrices $\mathbf{M}$ and $\mathbf{K}$ is not easily achievable. Thus, harmonic analysis seems the best option for addressing the solution to Eq. (38) with frequency-dependent parameters. However, as proved in this section, the harmonic solution can be significantly simplified by using some standard ingredients of modal analysis.

Moreover, the technique that we are describing in what follows allows circumventing the curse of dimensionality involved by the consideration of multiple parameters (grouped in vector $\boldsymbol{\mu}$) without requiring the affine decomposition described at the end of previous section, which remains in most cases a tricky issue.

For the sake of generality, we extend model (38) to the multi-parametric case, which now reads

$$\left(-\omega^2 \mathcal{L}^m(\boldsymbol{\mu}(\omega))\mathbf{M} + \mathcal{L}^k(\boldsymbol{\mu}(\omega))\mathbf{K}\right)\mathbb{U}(\omega,\boldsymbol{\mu}) = \mathbf{f} \tag{39}$$

We now consider matrix $\mathbf{P}$ diagonalizing matrices $\mathbf{M}$ and $\mathbf{K}$, that is,

$$\begin{cases} \mathbf{P}^\mathsf{T}\mathbf{M}\mathbf{P} = \mathbb{M} \\ \mathbf{P}^\mathsf{T}\mathbf{K}\mathbf{P} = \mathbb{K} \end{cases} \tag{40}$$

with $\mathbb{M}_{ij} = m_{ii}\delta_{ij}$ and $\mathbb{K}_{ij} = k_{ii}\delta_{ij}$, with δ_{ij} the Kroenecker's delta, i.e. $\mathbb{M}$ and $\mathbb{K}$ becomes diagonal with entries m_{ii} and k_{ii} respectively.

Such a choice implies that the system is no longer described in terms of its nodal degrees of freedom, but rather in terms of the modal content. The two are formally related through the linear transformation

$$\mathbb{U} = \mathbf{P}\boldsymbol{\xi} \tag{41}$$

Thus, the dynamical problem (39) reduces to

$$\left(-\omega^2 \mathcal{L}^m(\boldsymbol{\mu}(\omega))\mathbb{M} + \mathcal{L}^k(\boldsymbol{\mu}(\omega))\mathbb{K}\right)\boldsymbol{\xi}(\omega,\boldsymbol{\mu}) = \mathbf{P}^\mathsf{T}\mathbf{f} = \hat{\mathbf{f}} \tag{42}$$

which results in a system of N_n decoupled algebraic equations (N_n being the size of matrices $\mathbf{M}$, $\mathbf{C}$, and $\mathbf{K}$)

$$\left(-\omega^2 \mathcal{L}^m(\boldsymbol{\mu}(\omega))m_{ii} + \mathcal{L}^k(\boldsymbol{\mu}(\omega))k_{ii}\right)\xi_i(\omega,\boldsymbol{\mu}) = \hat{f}_i, \quad i = 1,2,\cdots,N_n \tag{43}$$

from which it results

$$\xi_i = \frac{\hat{f}_i}{\left(-\omega^2 \mathcal{L}^m(\boldsymbol{\mu}(\omega))m_{ii} + \mathcal{L}^k(\boldsymbol{\mu}(\omega))k_{ii}\right)}, \quad i = 1,2,\cdots,N_n \tag{44}$$

that allows reconstituting $\boldsymbol{\xi}$ and from it the nodal amplitudes from Eq. (41), i.e. $\mathbb{U} = \mathbf{P}\boldsymbol{\xi}$.
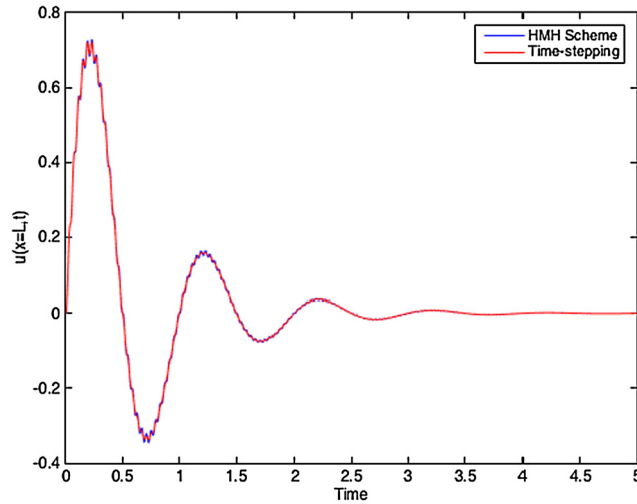
Fig. 1. Displacement at the rod end at which the prescribed force is applied, $u(x = L, t)$, computed by using time-stepping (red curve) and the HMH scheme (blue curve) for linear dynamics.

A separated representation can be derived by writing

$$\mathbb{U}(\omega, \boldsymbol{\mu}) = \sum_{k=1}^{N_n} \mathbf{Z}_k \xi_k(\omega, \boldsymbol{\mu}) \tag{45}$$

where $\mathbf{Z}_k$ is the k-column of matrix $\mathbf{P}$.

Now, as soon as the parameters are defined, the parametric scalars $\xi_k(\omega, \boldsymbol{\mu})$ are particularized, leading to $\mathbb{U}(\omega)$, which allows coming back to the time domain $\mathbf{U}(t)$ by applying an inverse Fourier transform according to Eq. (11).

This simple strategy for computing solutions of parametrized dynamics, with frequency-dependent parameters, proved to be, according to the authors' experience, more efficient than other existing strategies summarized in Section 2, with potential capabilities to compute under real-time constraints.

5. Numerical results

5.1. 1-D problem

In order to illustrate the capabilities of the proposed strategy, this section addresses the dynamics of the rod of length L, cross section A, clamped at its left boundary and subjected to an axial load applied on its right boundary, evolving in time according to $f(t) = \sin(2\pi t)e^{-1.5t}$. The one-dimensional mechanical response is computed from the discrete system

$$\mathbf{M}\frac{\mathrm{d}^2\mathbf{U}(t)}{\mathrm{d}t^2} + \mathbf{C}\frac{\mathrm{d}\mathbf{U}(t)}{\mathrm{d}t} + \mathbf{K}\mathbf{U}(t) = \mathbf{F}(t) \tag{46}$$

whose expression in the frequency domain is

$$\left(-\omega^2\mathbf{M} + \mathrm{i}\omega\mathbf{C} + \mathbf{K}\right)\mathbb{U} = \mathbf{f} \tag{47}$$

while assuming the proportional damping expressed by $\mathbf{C} = a_1\mathbf{K}$.

In the first analysis, the model parameters were selected according to: $\rho = 1$, $L = 1$, $A = 10^{-4}$, $E = 10^4$ and $a_1 = 10^{-4}$ (all the units are in the metric system). Then both formulations (46) and (47) were solved, the former by using a standard time-stepping technique (with time step $\Delta t = 10^{-4}$), whereas the latter was solved by the previously described HMH scheme. Fig. 1 compares both solutions and evidences that the one obtained by using the HMH scheme is more accurate for the considered time step. Obviously, by decreasing the time step, both solutions superpose, but the impact in computing time is significant. This is shown through the zoomed-in comparison in Fig. 2.

After proving that, in the linear case, both approaches lead to similar results, more complex behaviors were addressed by assuming a frequency-dependent damping. In the present case, the damping was modeled from

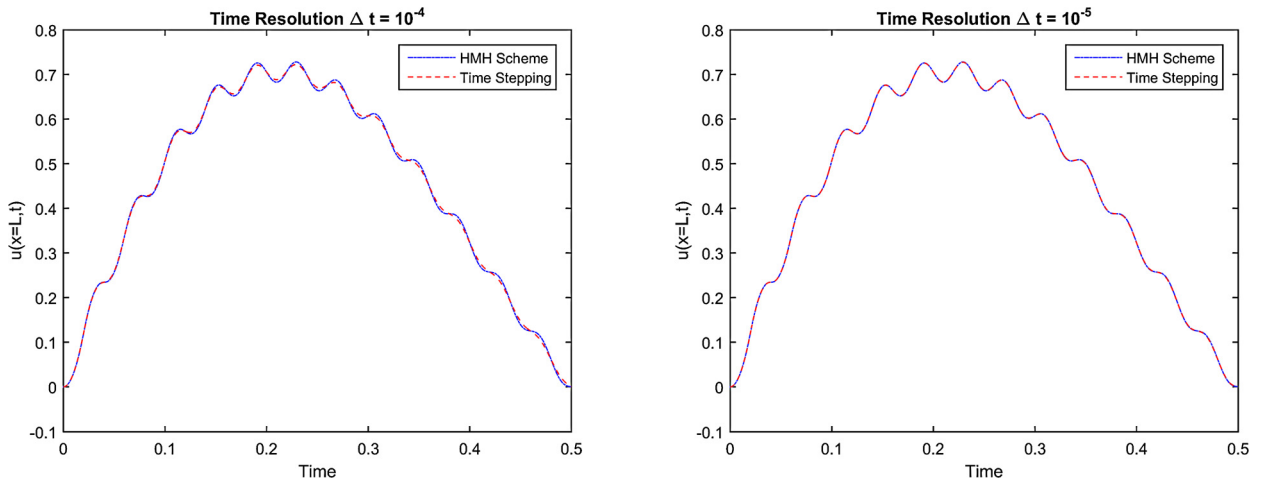$$\mathbf{C} = \frac{\eta(\omega)}{|\omega|}\mathbf{K} \tag{48}$$

Fig. 2. Displacement in rod at $x = L$, convergence of time stepping scheme to HMH solution with increase in time resolution from $\Delta t = 10^{-4}$ to 10^{-5}.
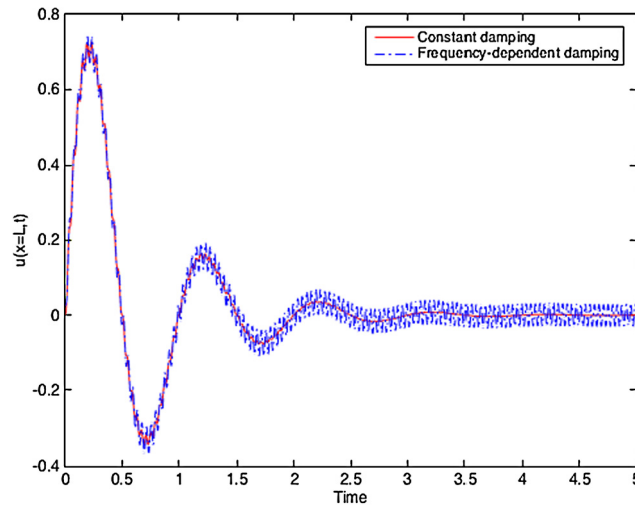

Fig. 3. Displacement at the rod end at which the prescribed force applies, $u(x = L, t)$, computed by using HMH scheme in the case of constant damping (red curve) and frequency-dependent damping (blue curve).

with

$$\eta(\omega) = (0.2\,\omega + 1) \times 10^{-4} \tag{49}$$

In the present case, the problem was solved in the frequency space by using the HMH scheme, but because it has not a time-description counterpart, the results were not compared with a reference time solution. Fig. 3 compares the solution provided by the HMH scheme when considering constant and frequency-dependent damping, after performing the inverse transform of the solutions obtained in the frequency domain. The significant effect of the frequency dependency of the damping can be noticed.

Finally, in order to prove the ability of addressing parametric models while considering frequency-dependent parameters, we addressed the just-discussed example, but now adding the Young modulus E as a parameter, and then the solution is searched under the parametric form $\mathbb{U}(\omega, E)$, with the damping depending on the frequency. The solution can be particularized for any value of the elastic modulus and pushed-back to the time domain. Fig. 4 depicts the recovered time-solutions for four different elastic moduli, from which an extremely high effect of the elastic modulus on the time-response can be noticed.

5.2. 2-D problem

To further prove the efficiency and capability of the method developed in the current study, a 2-D plane stress dynamic problem was also solved. A mesh on the geometry is presented in Fig. 5. The parameter values used in the solution to 2-D
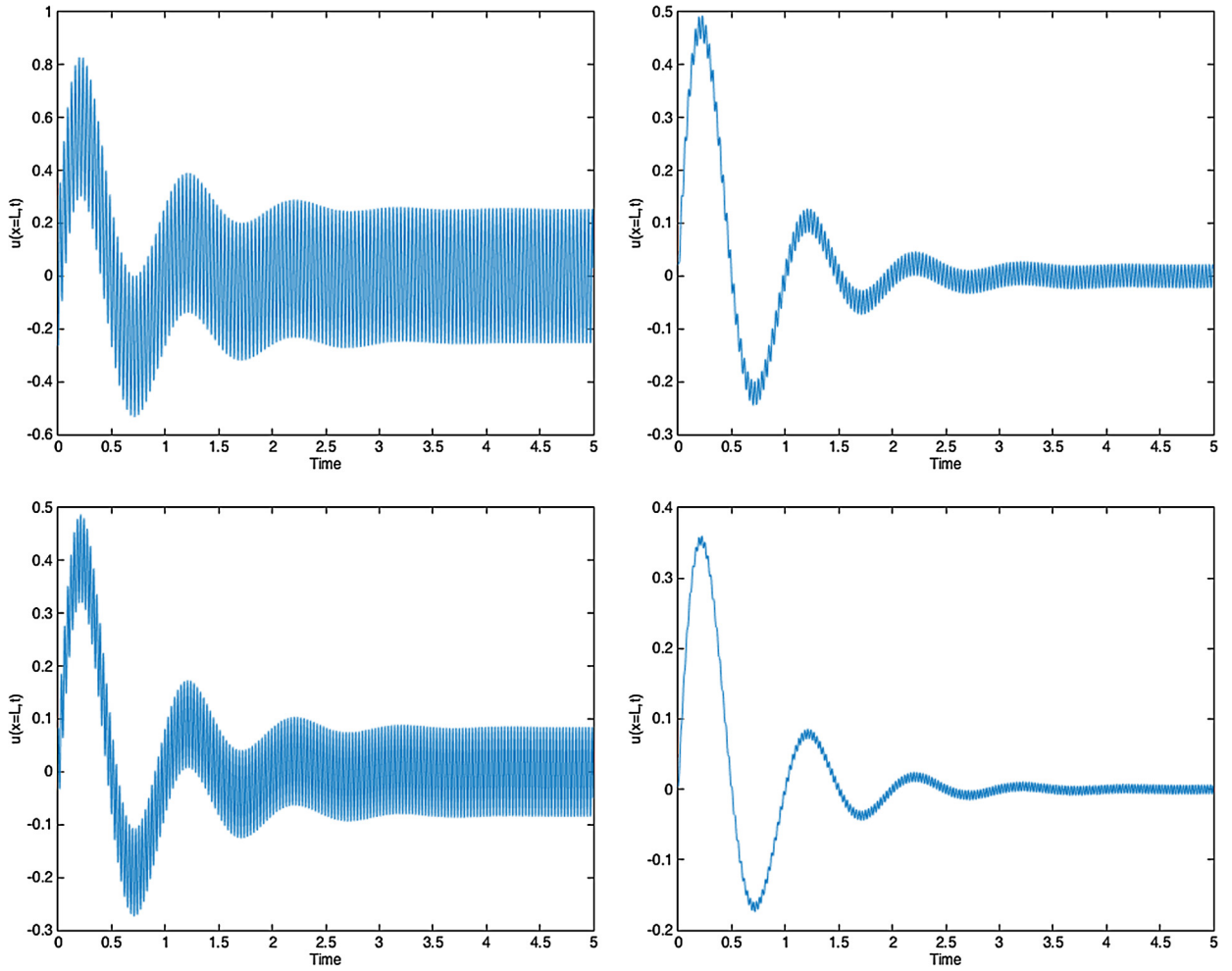
Fig. 4. Displacement at the rod end at which the prescribed force applies, $u(x = L, t)$, computed by using the HMH scheme in the case of frequency-dependent damping for four different elastic moduli: $E = 1.25 \times 10^4$ (top left), 1.5×10^4 (top right), 1.75×10^4 (bottom left), and 2×10^4 (bottom right).
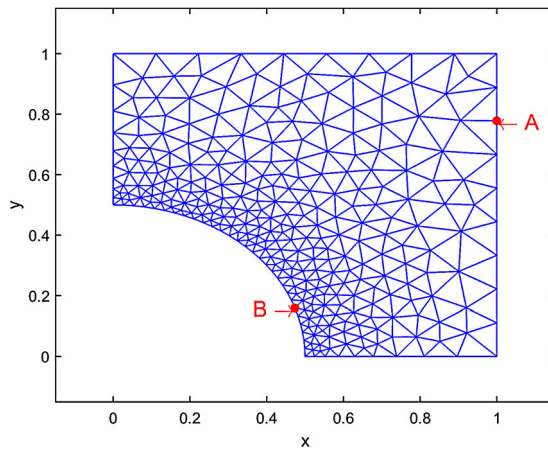

Fig. 5. Mesh for the 2-D plate with nodes 20 and 60 marked by A and B, respectively.

problem are: $E = 1 \times 10^4$, $\nu = 0.33$. The dimensions of the plate is 1 m×1 m, with a quarter of a circular hole of radius 0.5 m at the bottom left corner of the plate.
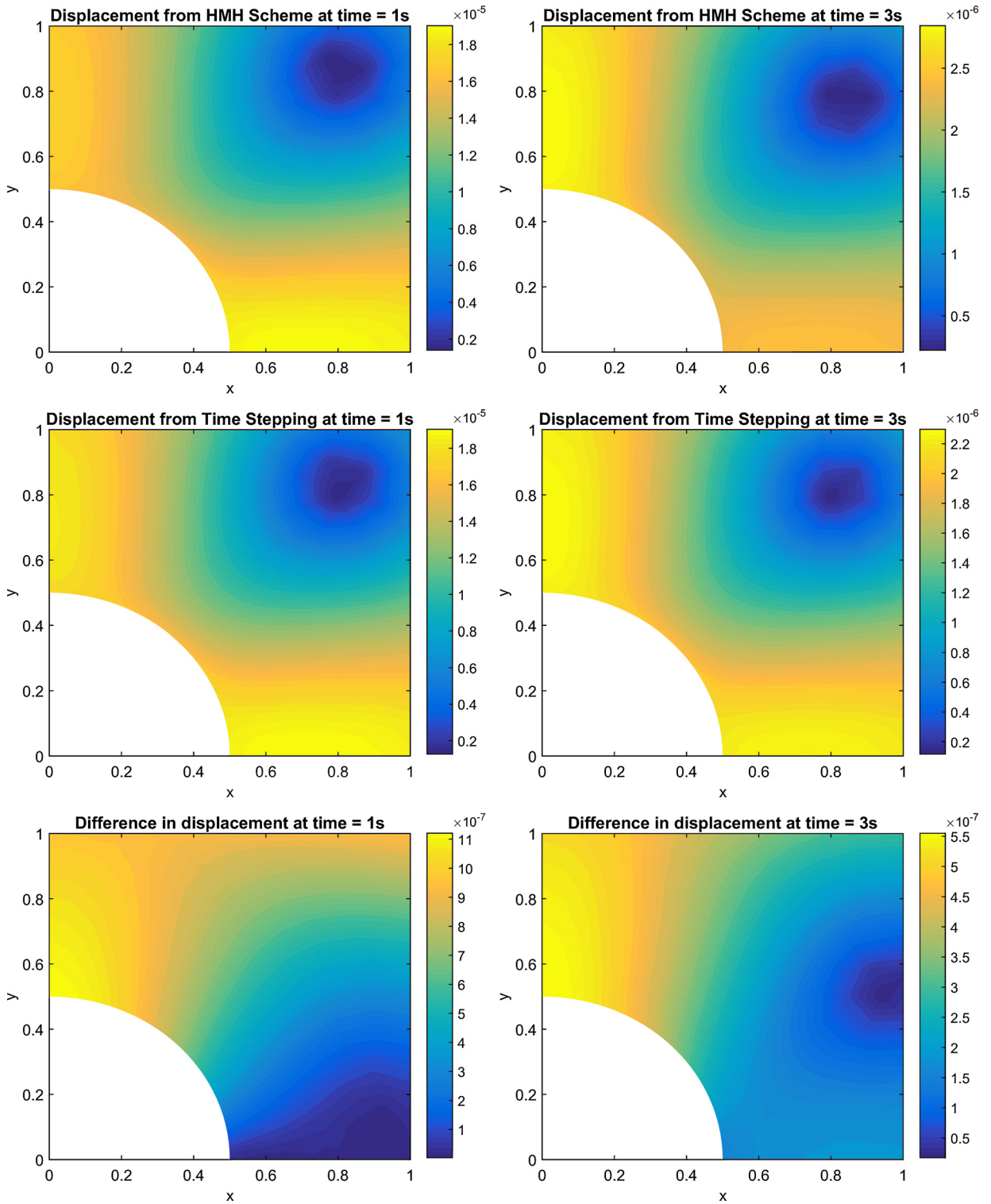
Fig. 6. Displacement field in the plate computed by using the HMH and time-stepping schemes and the difference between the two schemes at times $t = 1$ s (left column) and $t = 3$ s (right column).

The left and bottom edge of the plate are subjected to symmetric boundary conditions, i.e. $u(x = 0, y) = 0$ and $v(x, y = 0) = 0$, where u, v represent the x and y components of the displacement field, respectively. The right-hand edge of the plate is subjected to a uniform time varying load similar to the one presented in the 1-D case. The problem was
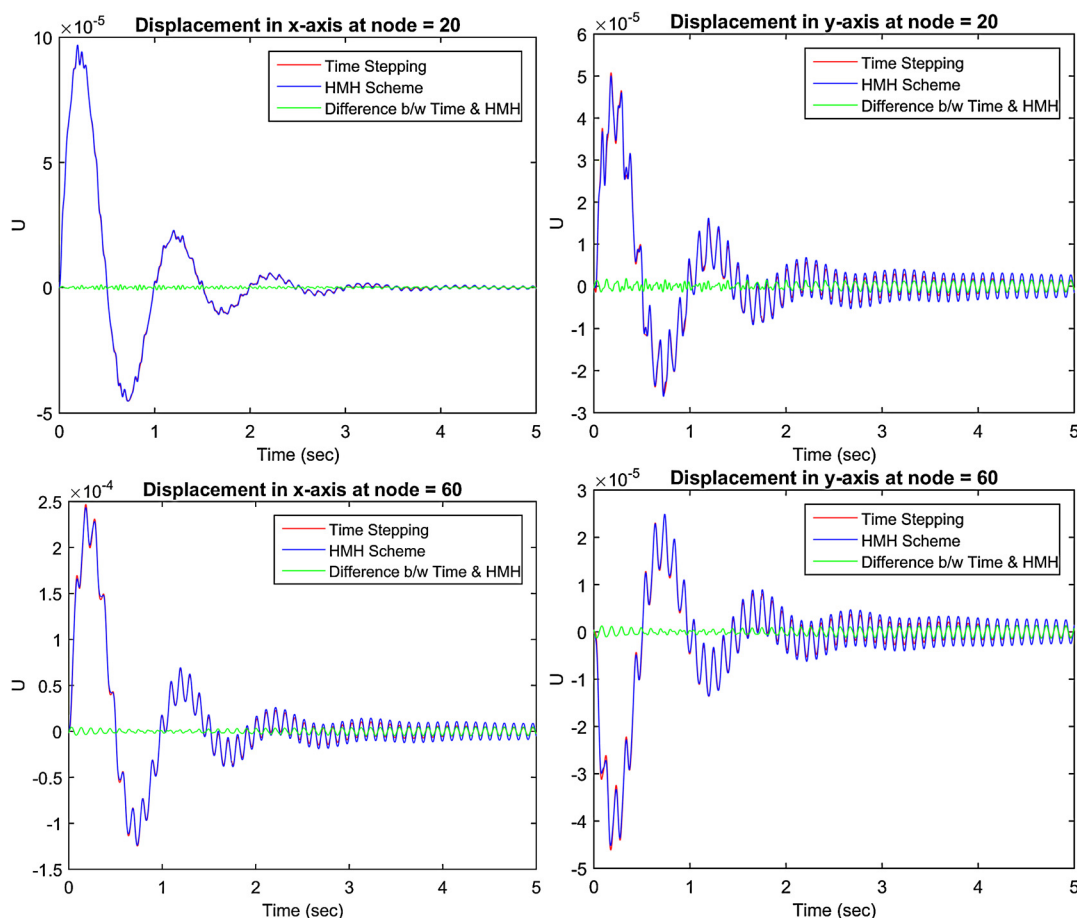
Fig. 7. Displacement components u and v at nodes marked A and B, located at the positions indicated in Fig. 5, computed by using the HMH and time-stepping schemes, and the difference between both solutions.

then solved using both HMH scheme and a time-stepping scheme with a time step of $\Delta t = 10^{-4}$. The results are presented in Fig. 6 in terms of contour plot at times $t = 1$ s and $t = 3$ s as well as the difference between the solutions of both schemes. Again, we observed that the HMH scheme is more accurate for the comparable time step in time domain solution. This has significant advantage in terms of saving computational time. The effectiveness of the method as compared with time-stepping scheme is presented for a couple of nodes in Fig. 7. It can be observed that the time-stepping scheme suffers from excessive numerical dissipation due to the first-order time-stepping scheme utilized.

6. Conclusions

In this work, we revisited the solution to elastodynamics while operating in the frequency domain. This formulation allows considering frequency-dependent parameters without major difficulties. Moreover,by virtue of the linearity of the problem, the time-solution can be reconstructed with no particular effort, potentially enabling real-time calculations. However, the main difficulty of such an approach lies in the difficulty of recovering an affine decomposition (separated form) for the discrete operators, which is the real bottleneck for efficient application of traditional model order reduction strategies. In this paper, we succeeded to define a hybrid technique combining the main ingredients of harmonic and modal analyses able to efficiently compute parametric solution within the framework of frequency-dependent parametric models.

References

[1] R.W. Clough, J. Penzien, Dynamics of Structures, Civil Engineering Series, McGraw-Hill, New York, 1993.
[2] S. Quraishi, C. Schroder, V. Mehrmann, Solution of large scale parametric eigenvalue problems arising from brake squeal modeling, Proc. Appl. Math. Mech. 14 (2014) 891–892.
[3] F. Tisseur, K. Meerbergen, The quadratic eigenvalue problem, SIAM Rev. 43 (2) (2001) 235–286.
[4] F.T. Hadjiioannou, T.A. Apostolatos, N.V. Sarlis, Sarlis stochastic parametric amplification due to higher order correlations: a perturbative approach to non-Abelian effects in time ordering, Phys. Rev. E 74 (051118) (2006), published 21 November 2006.
[5] M. Domaneschi, L. Martinelli, Refined optimal passive control of buffeting-induced wind loading of a suspension bridge, Wind Struct. 18 (2014) 1–20, https://doi.org/10.12989/was.2014.18.1.001.

[6] F. Chinesta, P. Ladeveze, E. Cueto, A short review on model order reduction based on proper generalized decomposition, Arch. Comput. Methods Eng. 18 (4) (2011) 395–404.

[7] F. Chinesta, A. Ammar, E. Cueto, Recent advances and new challenges in the use of the proper generalized decomposition for solving multidimensional models, Arch. Comput. Methods Eng. 17 (4) (2010) 327–350.

[8] F. Chinesta, A. Leygue, F. Bordeu, J.V. Aguado, E. Cueto, D. Gonzalez, I. Alfaro, A. Ammar, A. Huerta, Parametric PGD based computational vademecum for efficient design, optimization and control, Arch. Comput. Methods Eng. 20 (1) (2013) 31–59.

[9] F. Chinesta, R. Keunings, A. Leygue, The Proper Generalized Decomposition for Advanced Numerical Simulations, A Primer Springerbriefs, Springer, 2014.

[10] D. Borzacchiello, J.V. Aguado, F. Chinesta, Reduced order modelling for efficient numerical optimisation of a hot-wall chemical vapour deposition reactor, Int. J. Numer. Methods Heat Fluid Flow 27 (7) (2017) 1602–1622.

[11] A. Pecker, Dynamique des Sols, Presses de L'École Nationale des Ponts et Chaussées, Paris, 1984.

[12] S.H. Crandall, The role of damping in vibration theory, J. Sound Vib. 11 (1) (1970) 3–18.

[13] L. Boucinha, A. Ammar, A. Gravouil, A. Nouy, Ideal minimal residual-based proper generalized decomposition for non-symmetric multi-field models – application to transient elastodynamics in space-time domain, Comput. Methods Appl. Mech. Eng. 273 (2014) 56–76.

[14] A. Barbarulo, H. Riou, L. Kovalevsky, P. Ladeveze, PGD-VTCR: a reduced order model technique to solve medium frequency broad band problems on complex acoustical systems, J. Mech. Eng. 60 (5) (2014) 307–314.

[15] J.V. Aguado, A. Huerta, F. Chinesta, E. Cueto, Real-time monitoring of thermal processes by reduced order modelling, Int. J. Numer. Methods Eng. 102 (5) (2015) 991–1017.

[16] C. Germoso, J.V. Aguado, A. Fraile, E. Alarcon, F. Chinesta, Efficient PGD-based dynamic calculation of non-linear soil behavior, C. R. Mecanique 344 (2016) 24–41.

[17] S. Gregory, M. Tur, E. Nadal, J.V. Aguado, F.J. Fuenmayor, F. Chinesta, Fast simulation of the pantograph-catenary dynamic interaction, Finite Elem. Anal. Des. 129 (2017) 1–13.

[18] F. Chinesta, A. Ammar, A. Leygue, R. Keunings, An overview of the proper generalized decomposition with applications in computational rheology, J. Non-Newton. Fluid Mech. 166 (11) (2011) 578–592.

[19] F. Chinesta, A. Leygue, F. Bordeu, J.V. Aguado, E. Cueto, D. Gonzalez, I. Alfaro, A. Ammar, A. Huerta, PGD-based computational vademecum for efficient design, optimization and control, Arch. Comput. Methods Eng. 20 (1) (2013) 31–59.

[20] M. Barrault, Y. Maday, N.C. Nguyen, A.T. Patera, An 'empirical interpolation' method: application to efficient reduced-basis discretization of partial differential equations, C. R. Acad. Sci. Paris, Ser. I 339 (9) (2004) 667–672, https://doi.org/10.1016/j.crma.2004.08.006.

[21] S. Chaturantabut, D.C. Sorensen, Nonlinear model reduction via discrete empirical interpolation, SIAM J. Sci. Comput. 32 (5) (2010) 2737–2764.

[22] M.H. Malik, D. Borzacchiello, F. Chinesta, P. Diez, Inclusion of frequency-dependent parameters in power transmission lines simulation using harmonic analysis and proper generalized decomposition, Int. J. Numer. Model. (2018) e2331, https://doi.org/10.1002/jnm.2331.